Coastal Dynamics 2017
Paper No. 050

TILT CURRENT METERS IN THE SURF ZONE: BENCHMARKING UTILITY IN HIGH-FREQUENCY OSCILLATORY FLOW

Katherine Anarde[1] and Jens Figlus[2]

Abstract

Tilt current meters (TCMs) are a low-cost way of measuring stationary current velocities in coastal waters. In the nearshore environment, the combined influence of waves, wave breaking, and currents add complexity to the instrument response. This study explores the utility of TCMs in measuring near-bed flow velocities in the surf zone on a wave-dominated coast where turbulent bores, wave set-up, and alongshore currents dominate surf zone hydrodynamics. Initial field studies suggest that TCMs can be used to measure alongshore (low-frequency) currents during low wave energy conditions using standard tilt-to-speed calibration methods. Additionally, TCMs can resolve orbital wave motions; however, experiments within a controlled environment are needed to improve transfer function estimates relating tilt to velocity in highly energetic oscillatory flow.

Key words: field instrumentation calibration, waves, currents, nearshore flow measurements

1. Introduction

TCMs are designed to measure marine currents in accordance with the drag-tilt principle: within a stationary current flow, a tethered object will experience a tilt induced by the force balance of buoyancy, drag, and mooring tension. Local current velocity can then be related to tilt either by analytic approximation or empirically by comparison with a reference measurement. TCMs have been successfully deployed to measure unidirectional flows in rivers and slowly oscillating flows in tidally influenced bodies of water (Marchant et al., 2014; Lowell et al., 2015; Radermacher et al., 2015). In these studies, high frequency signals associated with wave motion, turbulence, and vortex shedding are removed either by averaging or through the use of low-pass filters. In the nearshore environment, TCM motion may cease to follow the stationary (or semi-stationary) current due to the added influence of orbital wave velocities. Therefore, the utility of TCMs in measuring current in the presence of waves, or conversely orbital wave velocities atop a stationary current, is contingent upon a clear understanding of the instrument frequency response for a range of wave conditions. If successfully validated for use in the nearshore, TCMs could be used to enhance the spatial resolution of field investigations, or to reduce the financial impact of instrument loss in high-risk environments given their relatively low cost compared to other current meters.

The objective of this study is to investigate the utility of TCMs in measuring near-bed flow velocities in shallow water (0.5 – 2.0 m) and high-frequency oscillatory flow. New field observations are presented relating TCM and co-located acoustic Doppler velocimeter (ADV) measurements within the inner surf zone on a wave-dominated coast during low and moderate wave energy conditions. Data analysis techniques are discussed in Section 2. Results from field studies are presented in Section 3 and then put into context of ongoing flume studies in Section 4.

1.1 Instrument Design

The TCMs used in this study are a prototype design by Lowell Instruments for use in shallow water. The instrument consists of a buoyant ellipsoid float surrounding a three-axis accelerometer and three-axis magnetometer within polyvinyl chloride housing. The total mass of the TCM is 233 g and the total length

[1]Department of Civil and Environmental Engineering, Rice University, Houston, Texas, U.S.A. kanarde@rice.edu
[2]Department of Ocean Engineering, Texas A&M University – Galveston Campus, Texas, U.S.A. figlusj@tamu.edu

(minus tether) is 23 cm. The TCM was initially calibrated by the manufacturer in a tow tank to empirically relate tilt to flow velocity. The instrument was anchored using an approximately 5-cm long tether and towed through fresh water in a series of tests with speeds ranging from 0 m/s to the tow tank maximum of 1 m/s. This data was corrected for salt-water density, low-pass filtered, and averaged to produce a tilt-to-speed calibration curve. The calibration curve was extrapolated beyond 1 m/s to the estimated maximum velocity of 2 m/s, which corresponds to a 90-degree tilt (Nick Lowell, personal communication).

Instrument mounts used in this study were optimized over a series of tests to minimize issues caused by scouring, sedimentation, and overturning. The final design consists of the TCM anchored to a low-profile concrete base plate via a spliced nylon tether rope, which is secured underneath the mount by a shackle. A pressure transducer is mounted to the side of the base plate to track submergence of the instrument and measure wave conditions (Figure 1).

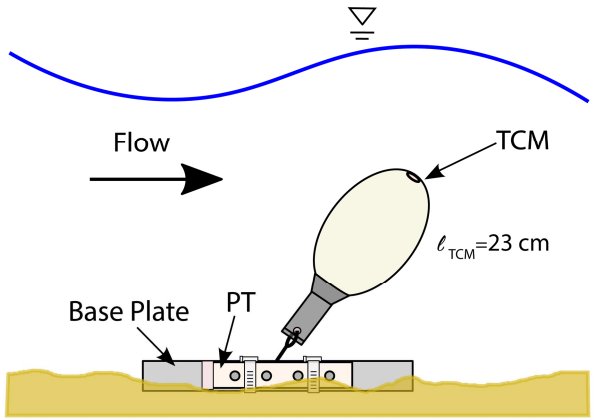

Figure 1. Schematic of the instrument pod design consisting of a moored tilt current meter (TCM) and side-mounted pressure transducer (PT).

1.2 Field site and data collection

Data were collected over two deployments representative of low and moderate wave-energy conditions at Galveston Island State Park, Texas, U.S.A. This portion of the upper Texas Gulf coast is a wave-dominated, micro-tidal environment with a semi-diurnal tidal regime and mean tidal range of 0.35 m (NOAA, 2017). Galveston Island State Park is a low gradient ($\beta \approx 0.008 - 0.011$), dissipative beach characterized by several pronounced bars and troughs composed of very fine sand (d_{50} = 0.13 mm) (Rogers and Ravens, 2008). The dominant wind and wave direction is from the SSE, resulting in an alongshore current directed to the W and SW. However, shifts in direction of the alongshore current towards the E and NE due to local changes in wind and wave direction have been observed as well. During the winter months, cold fronts that pass through the region can generate dramatic increases in wind speed (>10 m/s) and rapid shifts in wind direction (180 deg). These events are characterized by a pre-frontal phase of high-energy southerly winds followed by a rapid shift to winds from the N or W after the passage of the cold front (Carlin et al., 2016).

Instrument setup, measurement location, and data collection parameters were consistent between deployments. Accelerometer (TCM), velocity (ADV), and pressure observations were logged continuously at 16 Hz. The ADV/TCM instrument pairs were situated between the beach step and the first sand bar with approximately 1 m of separation. While only a single pair of instruments is discussed here, 7 instrument pods were deployed in a cross-shore array extending ~100 m into the surf zone during both deployments. The ADVs were mounted downward looking on a temporary scaffold frame with the sampling volume located approximately 25 cm above the bed.

2. Data Processing and Analysis

The results in this paper were produced from 32,768 continuous samples (~34 min) recorded over a single

tidal cycle within one hour of high tide. Over this time, the data are considered stationary as changes in water levels, due to the influence of tidal oscillations, and wave statistics were small. Potentially inaccurate individual ADV velocity estimates were identified from low along-beam signal-to-noise ratios (SNR) and low along-beam correlations. The coherence between pressure and orbital wave velocity time series (C_{pu}) over the wind sea-swell frequency band ($0.07 < f < 0.85$ Hz, Figure 2) was additionally used to identify corrupted sample windows (Elgar et al., 2005). The ADV quality control thresholds used for data rejection in this study were $C_{pu} < 0.9$, SNR < 10 dB, and along-beam correlations < 62%.

TCM accelerometer measurements were converted to tilt angle for each discrete time n as

$$\theta(n) = \cos^{-1}\left(\frac{\boldsymbol{a}\cdot\boldsymbol{a_0}}{\|\boldsymbol{a}\|\|\boldsymbol{a_0}\|}\right) \tag{1}$$

with adjustment for non-zero acceleration ($\boldsymbol{a_0}$) at rest (Marchant et al., 2014). Tilt measurements were then screened for potential corruption by detritus, fish, turbulence, and partial submergence during passage of a wave trough. The TCM quality control procedures developed for this study utilize the probability density of the "whitened" data record to detect departures from stationarity. If it is assumed that the ~34 min tilt time series was generated by an autoregressive process,

$$X_n = \sum_{j=1}^{N} a_j X_{n-j} + \eta_n \tag{2}$$

where η_n is white noise, then the Yule Walker equations can be used to estimate the coefficients a_j from the power spectrum. The coefficients are incorporated into the design of a finite impulse response (FIR) filter of N terms, which when convolved with the original time series gives the "innovation" of X_n,

$$\eta_n = X_n - \sum_{j=1}^{N} a_j X_{n-j} \ . \tag{3}$$

This new series approximates white noise, meaning that it represents the residual signal that is statistically independent from the preceding time series (Kleiner and Martin, 1979). A robust weighted least-squares fit to the mean of the whitened time series is used to classify outliers as samples that differ from the mean by more than three standard deviations. This method offers an improvement over traditional outlier detection

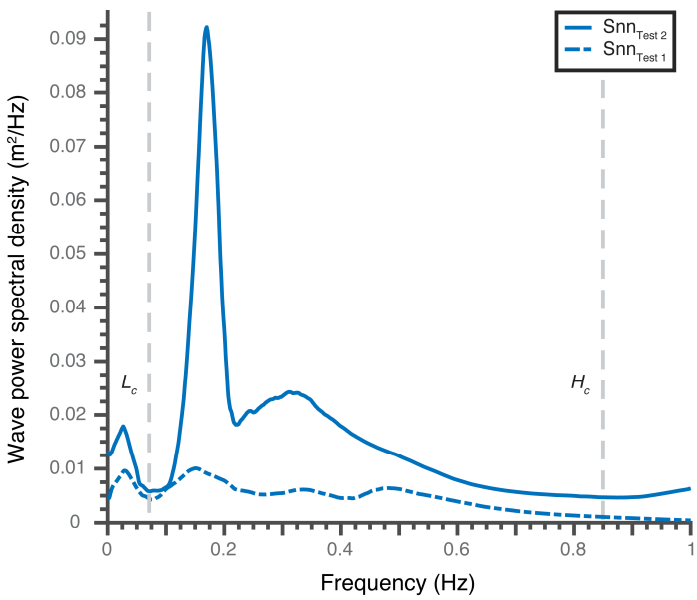

Figure 2. Wave power spectral density for Test 1 (current-dominated regime) and Test 2 (wave-dominated regime) labeled with the low (L_c = 0.07 Hz) and high (H_c = 0.85 Hz) cutoff frequencies chosen for this study. The sea-swell ($L_c < f < H_c$) significant wave heights calculated for Test 1 and Test 2 were 0.25 m and 0.46 m for a mean water depth of 0.86 m and 0.88 m, respectively.

algorithms tested on TCM tilt data (e.g. density and median filters) in that outliers are down-weighted when estimating the mean and standard deviation, resulting in improved retention of "good" data. Full data runs (~34 min windows) were rejected if the mean water depth, derived from the hydrostatic pressure recorded by the collocated pressure transducer, was less than 0.2 m above the TCM.

Outliers identified in the TCM and ADV time series were replaced with interpolated values using a cubic Hermite spline. When utilized, zero-phase low-pass filters were applied to each orthogonal component of acceleration (TCM) and velocity (ADV) separately, as each is a vector quantity.

Pressure measurements were corrected for local variations in atmospheric pressure and then transformed to wave power spectra using a robust power spectral density (PSD) estimator, discussed below. Water surface elevation spectra were corrected for depth attenuation of the pressure signal using linear wave theory and poro-elastic theory to account for burial of the pressure sensor (Raubenheimer et al., 1998). Wave statistics (wave height and period) were calculated for the infragravity ($0.005 < f < 0.07$ Hz) and wind sea-swell ($0.07 < f < 0.85$ Hz) frequency bands for both deployments. The high frequency cutoff of 0.85 Hz was selected by finding the last local minimum in the attenuation-corrected elevation spectra before rising to infinity; at this location, the pressure signal was at least three orders of magnitude higher than the instrument noise floor and the frequency was 5 times greater than the peak frequency (Smith, 2002; Jones and Monismith, 2007). To remove tidal signals from the data, the lower limit of the infragravity band was set to 0.005 Hz. The upper limit of the infragravity band was chosen based on the observed separation of energy between the incident wave band at 0.07 Hz (Figure 2).

Current velocity and wave power spectra were generated using an adaptive sine multitaper PSD estimator (Barbour and Parker, 2014). This method allows the number of tapers to vary with spectral shape resulting in resolution and accuracy that varies with frequency. The resulting spectral estimate yields significantly lower variance and enhanced resolution at low frequencies in comparison to less sophisticated windowing methods (e.g. Welch's method). Before estimating the spectrum, time series are linearly detrended and then prewhitened (described above) using a 4th order FIR filter to minimize spectral leakage (Kleiner and Martin, 1979). Frequency resolution and uncertainty (one-standard deviation errors) are estimated from the number of degrees of freedom, which is twice the number of tapers employed. The smoothness of the PSDs presented herein is not the result of ad-hoc post-processing but rather a product of the optimal variance reduction achieved by bandwidth-adaptive averaging of many tapers.

3. Results

3.1 Current dominated regime

The goal of the first field study ("Test 1") was twofold: 1) to assess the performance of the TCMs in the surf zone during a current dominated regime (low orbital wave velocities, spilling breakers), and 2) evaluate the influence of tether length on measured tilt. Test 1 occurred on October 8-9, 2016 during relatively low wave energy conditions: the sea-swell (H_{SS}) and infragravity significant wave heights (H_{inf}) at high tide, for a mean water depth of 0.86 m, were 0.25 m and 0.09 m with peak periods of 6.6 s and 34.7 s, respectively (Figure 2). The maximum ~34 min mean alongshore (SW), cross-shore, and vertical current velocities recorded by the ADV were 0.33, 0.16, and 0.10 m/s, respectively. The maximum instantaneous horizontal velocity recorded during this window was 0.78 m/s. Preliminary field investigations revealed that sediment accumulation atop the concrete pad over a single tidal cycle could exceed 5 cm within the inner surf zone, rendering the TCM immobile. To accommodate sedimentation and settling of the mount, the tether length was extended to 11.5 and 14.5 cm, as measured above the concrete pad. Upon retrieval of the instruments on October 9, less than 3 cm of sediment had accumulated atop each pad.

The coherence (the magnitude of the normalized cross-spectrum) between TCM tilt and ADV speed is greater than 0.90 below 0.01 Hz for both TCMs with the shorter tether slightly outperforming the longer tether (Figure 3). A sample density plot of tilt versus speed, shown for the 11.5 cm tether in Figure 4A, reveals that the data are well described by the manufacturer supplied tilt-to-speed calibration curve. When both time series are zero-phase low-pass filtered (corner frequency = 0.04 Hz), the trend deviates from the calibration and becomes more linear (Figure 4B and 4C). However, for the 11.5 cm tether, the calibration

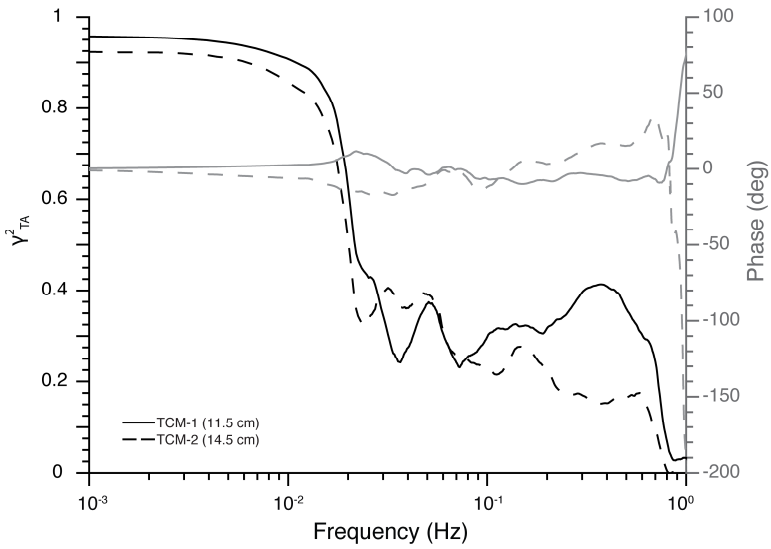

Figure 3. Coherence (γ_{TA}^2) and phase between TCM tilt and ADV speed during Test 1 (current dominated regime) for tethers of two different lengths: 11.5 and 14.5 cm. Spectral estimates are from ~34 min long time series at high tide sampled at 16 Hz with ADV (TCM) max $\pm 1\sigma$ = 1.85E-01 m/s (3.26E+02 deg) and min $\pm 1\sigma$ = 1.00E-06 m/s (1.83E-03 deg) errors.

curve still crosses the data in the area of the highest density of low frequency measurements ($\theta \approx 15°$, v ≈ 0.33 m/s). Using this calibration curve, tilt was converted to speed and then decomposed into alongshore and cross-shore components using the magnetometer heading and strike of the coastline. Figure 5 shows that TCM and ADV velocity spectra are highly coherent ($\gamma_{T_1A}^2 > 0.95$) for the 11.5 cm tether below 0.015 Hz in the alongshore direction with a constant phase near zero.

The standard model for the transfer function ($R_{TA}(f)$) where output is linearly related to input, but with additive noise, is given by

$$S_{TCM}(f) = R_{TA}(f)\, S_{ADV}(f) + \eta \tag{4}$$

where S_{TCM} and S_{ADV} are the complex Fourier coefficients of the TCM and ADV signals, respectively, and η is uncorrelated noise in the TCM record. This model is only applicable if the ADV record is assumed noise free, which is plainly inappropriate for the environment tested here. However, in the alongshore direction the coherence approaches unity at very low frequencies, which implies that if (4) holds, η is negligible. Thus, in this range, the modulus of the transfer function is given by the gain: for f = 0.004 Hz, $\gamma_{T_1A}^2$ = 0.9851, and $|R_{TA}|$ = 0.8234.

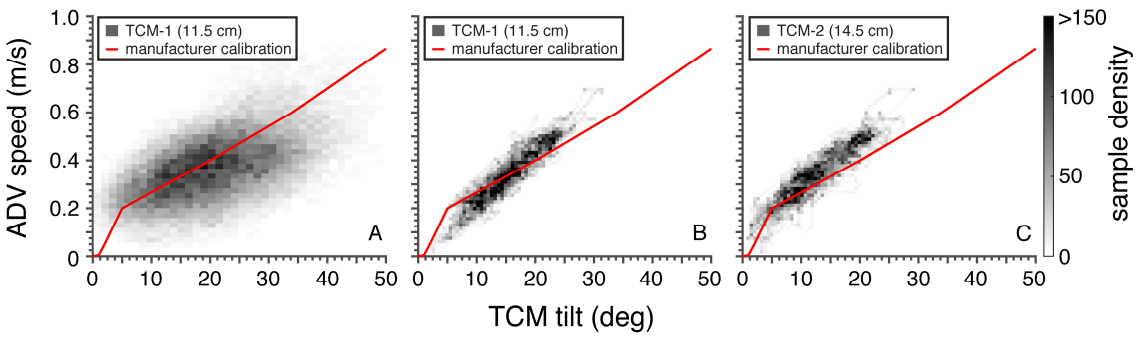

Figure 4. Density plots of TCM tilt versus ADV speed during Test 1 (current dominated regime, ~34 min window at high tide). Panel A: all frequencies (11.5 cm tether length only). Panel B: low frequencies (11.5 cm tether length; corner frequency = 0.04 Hz). Panel C: low frequencies (14.5 cm tether length; corner frequency = 0.04 Hz).

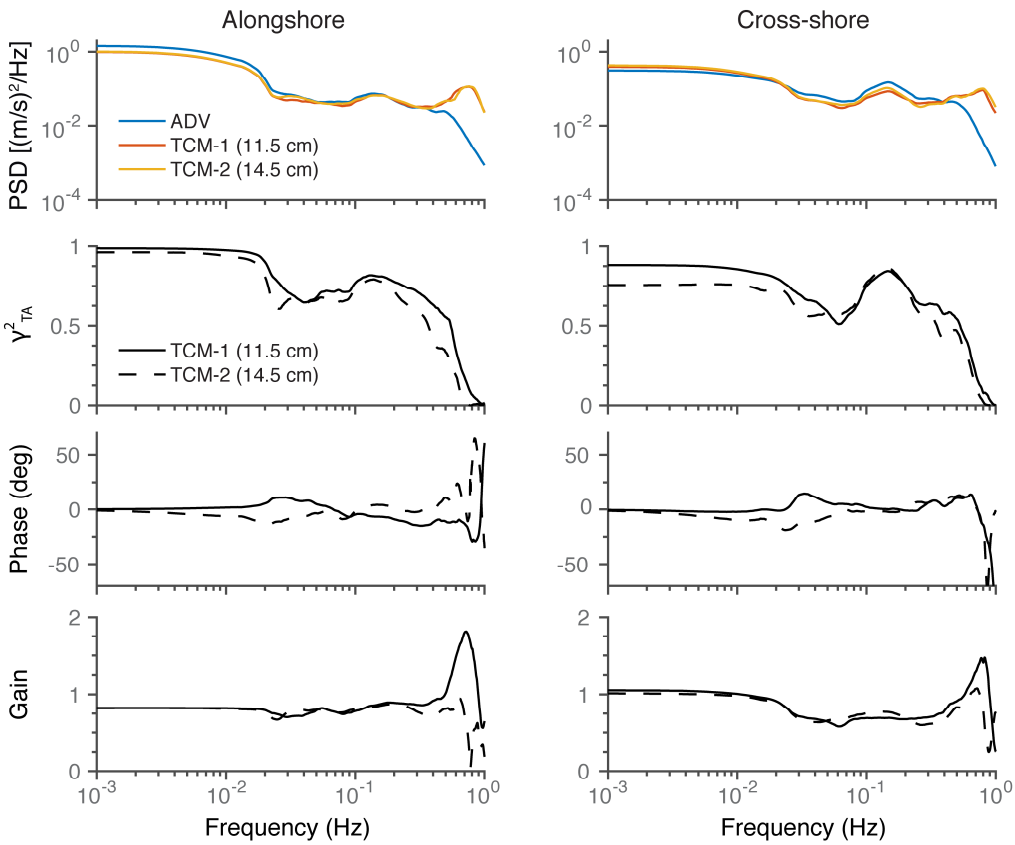

Figure 5. Velocity power spectral density, coherence, phase, and gain (transfer function amplitude) between TCM and ADV alongshore and cross-shore velocity components during Test 1 (current dominated regime). Tilt was transformed to velocity for both TCMs (11.5 and 14.5 cm tether) using the manufacturer supplied calibration curve. Spectral estimates are from ~34 min long time series at high tide sampled at 16 Hz with ADV (TCM) max $\pm 1\sigma$ = 3.43E-01 m/s (2.37E-01 m/s) and min $\pm 1\sigma$ = 1.32E-06 m/s (4.15E-07 m/s) errors.

Coherence is also high for the peak that appears in the frequency range 0.08 – 0.20 Hz in the cross-shore component, which is associated with incident sea-swell waves. Here, the longer tether ($\gamma^2_{T_2A}$= 0.8598) slightly outperforms the shorter tether ($\gamma^2_{T_1A}$ = 0.8441) in capturing orbital wave velocities. The prominent peak in the TCM spectrum in the band 0.5 – 1.0 Hz is interpreted as an instrument resonance since it clearly diverges from the ADV spectrum as it approaches its noise floor. This peak is of nearly equal amplitude for both components of TCM velocity, and in the cross-shore direction it is of nearly equal amplitude to the incident wave peak.

3.2 Wave dominated regime

The goal of the second field study ("Test 2") was to observe the performance of the TCMs in highly oscillatory flow where orbital wave velocities surpass alongshore current velocities. Test 2 occurred on November 17-18, 2016, during the pre-frontal phase of a cold front. At high tide, winds from the SSE exceeded 6 m/s with H_{SS} = 0.46 m (T_p = 5.89 s) and H_{inf} = 0.12 m (T_p = 37.9 s) for a mean water depth of 0.88 m (Figure 2). The maximum ~34 min mean alongshore (NE), cross-shore, and vertical current velocities recorded by the ADV were 0.39, 0.48, and -0.02 m/s, respectively. The maximum instantaneous horizontal velocity recorded during this window was 1.44 m/s. The 14.5 cm long tether was employed for Test 2 as it was hypothesized that the effective length of the tether would be substantially reduced by sediment accretion atop the mount. This was substantiated by an observed accumulation of ~3 cm within an hour of deployment (3 hours prior to high tide). When the instruments were inspected the following day, 10 cm of sediment had accumulated atop the concrete pad, however the mobility of the TCM did not

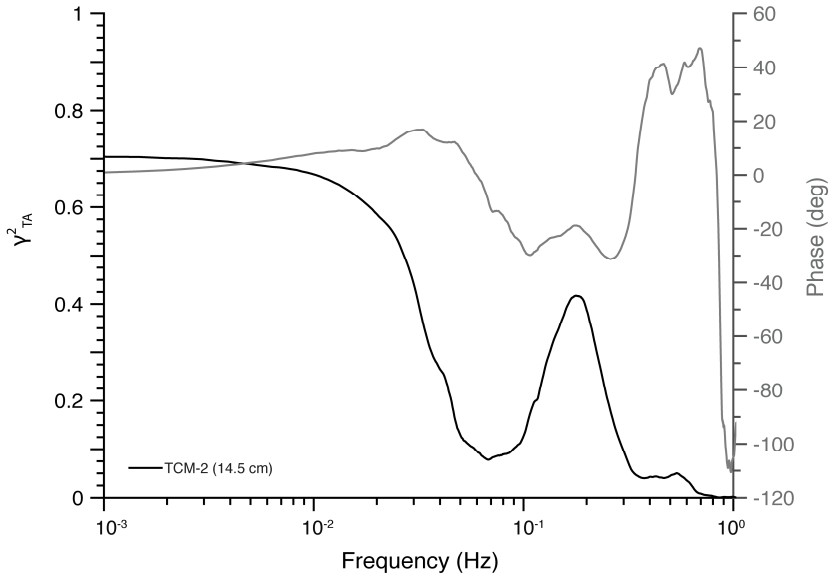

Figure 6. Coherence (γ^2_{TA}) and phase between TCM tilt (14.5 cm tether) and ADV speed during Test 2. Spectral estimates are from ~34 min long time series at high tide sampled at 16 Hz with ADV (TCM) max $\pm 1\sigma$ = 2.89E-02 m/s (9.26E+1 deg) and min $\pm 1\sigma$ = 4.69E-06 m/s (2.44E-02 deg) errors.

appear impaired. It is unclear if the total change in bed level occurred continuously over the deployment or if it was the result of a few large waves.

The coherence between TCM tilt and ADV speed during Test 2 was less robust than Test 1 with γ^2_{TA}< 0.71 below 0.01 Hz (Figure 6). While the density plot of tilt versus speed shows clustering of data around the manufacturer calibration curve for all frequencies (Figure 7A), the low-pass filtered data reveal that tilt measurements for low frequency signals correspond with higher velocities than predicted by the calibration curve and show less variance than observed during Test 1 (Figure 7B). This lack of correlation at low frequencies is also observed in the alongshore (γ^2_{TA} < 0.77) and cross-shore spectra (γ^2_{TA} < 0.55) below 0.015 Hz (Figure 8). Phase increases from 0 degrees with a linear slope (when plotted on a linear axis) up to ~0.05 Hz in both the cross-shore and alongshore directions.

Again, coherence is relatively high in the cross-shore component in the incident sea-swell wave band 0.08 – 0.22 Hz: γ^2_{TA} = 0.8621 for f = 0.163 Hz, which is a slightly higher peak frequency than that measured by the pressure transducer (Figure 2). The two signals are out of phase by -20 degrees over this band with a gain near unity. The peak power within the incident wave band during Test 2 is over double the magnitude of Test 1 (as recorded by the ADV) thus supporting the relative classification of the two deployments as moderate and low wave energy events, respectively. Beyond 0.22 Hz, the coherence

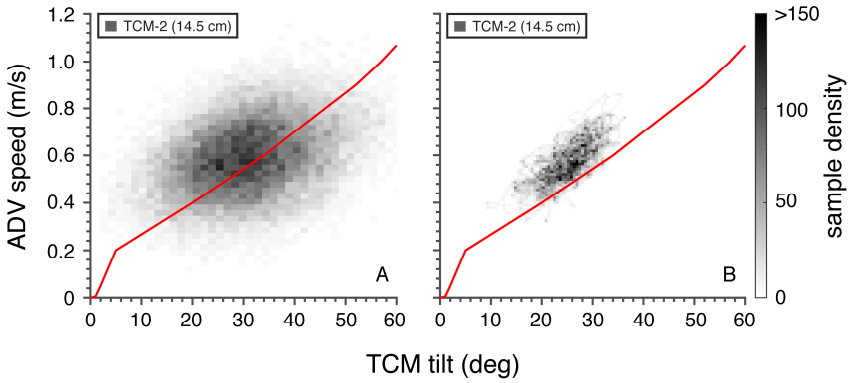

Figure 7. Density plots of TCM tilt versus ADV speed during Test 2 for the 14.5 cm tether. Panel A: all frequencies. Panel B: low frequencies (corner frequency = 0.04 Hz).

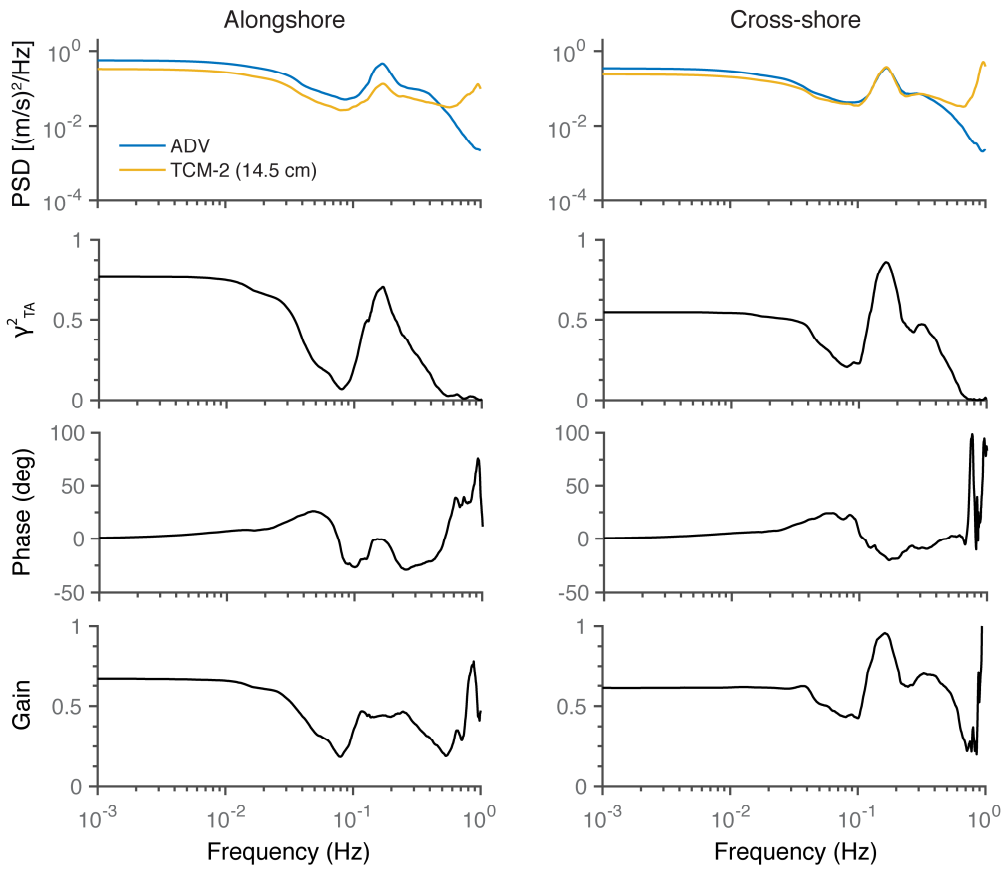

Figure 8. Velocity power spectral density, coherence, phase, and gain between TCM (14.5 cm tether) and ADV alongshore and cross-shore velocity components during Test 2. Tilt was transformed to velocity using the manufacturer supplied calibration curve. Spectral estimates are from ~34 min long time series at high tide sampled at 16 Hz with ADV (TCM) max $\pm 1\sigma$ = 5.60E-02 m/s (5.35E-02 m/s) and min $\pm 1\sigma$ = 5.55E-06 m/s (2.04E-05 m/s) errors.

plummets as the TCM resonance oscillation at ~1 Hz overtakes the linear instrument response. The power of this oscillation (0.9731 $(m/s)^2/Hz$) surpasses that of the incident wave signal captured by the TCM (0.3725 $(m/s)^2/Hz$).

4. Discussion and Future Work

A prototype TCM for use in shallow water was tested in the surf zone during low and moderate wave energy conditions. In the current dominated regime (Test 1), TCM tilt was highly coherent with ADV speed (Figure 3), with a near linear trend observed between tilt and speed for f < 0.04 Hz (Figure 4). When tilt was transformed to alongshore velocity using the manufacturer supplied preliminary calibration curve, the coherence approached unity for the 11.5 cm tether whereas the 14.5 cm tether was slightly less coherent (Figure 5). The cause of this discrepancy is visible in Figure 4C: the small increase in tether length (3 cm) decreases the tilt for the same speed at low frequencies. While this result is not entirely surprising, it illuminates the need for a clear understanding of how sediment accumulation atop the instrument mount affects the effective tether length. This could be accomplished by collocating the TCM with a bed-level sensor that can track elevation changes throughout an event. Appropriate tilt-to-speed calibration curves will need to be developed and tested for tether lengths suitable for applications where substantial bed-level changes are expected.

TCM motion is influenced by orbital wave velocities, as evidenced by relatively high coherence over the incident wave band during both deployments ($\gamma_{TA}^2 \approx 0.86$, Figures 5 and 8). However, it is unclear if the single tilt-to-speed curve is an appropriate method of calibration in high oscillatory flow. The lack of

coherence between tilt and speed during moderate wave energy conditions (Test 2, Figure 6) may be the result of noise, the relative strength of the resonant TCM oscillation (potentially driven by vortex shedding), inertia of the instrument, spatial variability of currents and waves in the inner surf zone, localized turbulence, or bed level changes (among others). The location and water depth chosen for both studies make it particularly challenging to isolate the sources of this incoherence as this environment is exposed to a range of hydrodynamic processes: offshore directed flow (undertow), orbital wave velocities, alongshore currents, and turbulent bores.

The results of these initial field studies suggest that TCMs can be a useful tool for measuring alongshore (low-frequency) currents in the surf zone during low wave energy conditions with appropriate calibration for variable effective tether length over the course of a deployment. For more energetic wave conditions, additional investigation on the utility of TCMs in measuring orbital wave velocities, or conversely current in the presence of waves is needed; this field study implies that further understanding of the TCM response will require testing in a controlled environment. The authors will continue to explore the utility of TCMs in highly energetic and oscillatory flow using a moveable bed wave flume and three-dimensional wave tank. If successfully validated, the TCMs will be used as part of a rapid response instrument array designed to measure nearshore and overland flow dynamics on barrier islands during extreme storms.

Acknowledgements

Ms. Anarde was supported by the Link Ocean Engineering and Instrumentation PhD Fellowship Program during this project. This study was supported in part by an Institutional Grant (NA14OAR4170102) to the Texas Sea Grant College Program from the National Sea Grant Office, National Oceanic and Atmospheric Administration, U.S. Department of Commerce, Texas A&M University at Galveston, and Rice University. The authors received additional support from the National Science Foundation under Grant No. OISE-1545837. We thank our undergraduate student researchers who assisted us in the field: Bryan Hunter Myers, Mick Prouse, and Connie Do.

References

Barbour, A.J., Parker, R.L., 2014. psd: Adaptive, sine multitaper power spectral density estimation for R. *Computers & Geosciences*, 63: 1–8. doi:10.1016/j.cageo.2013.09.015

Carlin, J.A., Lee, G.-H., Dellapenna, T.M., Laverty, P., 2016. Sediment resuspension by wind, waves, and currents during meteorological frontal passages in a micro-tidal lagoon. *Estuarine, Coastal and Shelf Science*, 172: 24–33. doi:10.1016/j.ecss.2016.01.029

Elgar, S., Raubenheimer, B., Guza, R.T., 2005. Quality control of acoustic Doppler velocimeter data in the surfzone. *Meas. Sci. Technol.*, 16, 1889. doi:10.1088/0957-0233/16/10/002

Jones, N.L., Monismith, S.G., 2007. Measuring short-period wind waves in a tidally forced environment with a subsurface pressure gauge. *Limnolology and Oceanography: Methods*, 5: 317–327.

Kleiner, B., Martin, R.D., 1979. Robust estimation of power spectra. *Journal of the Royal Statistical Society*, 41(3): 313–351. doi:10.2307/2985062

Lowell, N.S., Walsh, D.R., Pohlman, J.W., 2015. A Comparison of tilt current meters and an acoustic Doppler current meter in Vineyard Sound, Massachusetts. In *Current, Waves and Turbulence Measurement (CWTM) Proceedings*, 11th IEEE/OES Conference, pp. 1–7. doi:10.1109/cwtm.2015.7098135

Marchant, R., Stevens, T., Choukroun, S., Coombes, G., Santarossa, M., Whinney, J., Ridd, P., 2014. A buoyant tethered sphere for marine current estimation. *IEEE J. Oceanic Eng.*, 39(1): 2–9. doi:10.1109/JOE.2012.2236151

National Oceanic and Atmospheric Administration (NOAA), 2017. *Tides & Currents: Station 8771341 Galveston Bay Entrance, North Jetty, Texas*. https://tidesandcurrents.noaa.gov/ (accessed March 20, 2017).

Radermacher, M., Thackeray, Z.H., De Schipper, M., Gordon, L., Chrystal, C., Leuci, R., Reniers, A., 2015. Tilt current meter array: Field validation. In *E-proceedings of the 36th IAHR World Congress*, Den Haag, Netherlands.

Raubenheimer, B., Elgar, S., Guza, R.T., 1998. Estimating wave heights from pressure measured in sand bed. *J. Waterway, Port, Coastal, Ocean Eng.*, 124(3): 151–154. doi:10.1061/(ASCE)0733-950X(1998)124:3(151)

Rogers, A.L., Ravens, T.M., 2008. Measurement of longshore sediment transport rates in the surf zone on Galveston

Island, Texas. *Journal of Coastal Research*, 2(2B): 62–73. doi:10.2112/05-0564.1
Smith, J., 2002. Wave pressure gauge analysis with current. *Journal of Waterway, Port, Coastal, and Ocean Engineering*, 128(6), 271–275.